J. Anat. (2007) **210**, pp703–722 doi: 10.1111/j.1469-7580.2007.00725.x

Craniofacial growth in fetal *Tarsius bancanus*: brains, eyes and nasal septa

Nathan Jeffery,[1] Karen Davies,[2] Walter Köckenberger[3] and Steve Williams[2]

[1]*Division of Human Anatomy & Cell Biology, School of Biomedical Sciences, University of Liverpool, UK*
[2]*Imaging Science and Biomedical Engineering, University of Manchester, UK*
[3]*Sir Peter Mansfield Magnetic Resonance Centre, School of Physics and Astronomy, University of Nottingham, UK*

Abstract

The tarsier skull has been of particular interest in studies of primate taxonomy and functional morphology for several decades. Despite this, there remains no comprehensive data on how the tarsier skull develops, especially in relation to the soft-tissues of the head. Here we have documented for the first time fetal development of the skull and brain as well as the nasal septum and eyes in *T. bancanus*. We have also tested for the possible influence of these tissues in shaping skull architecture. Nineteen post-mortem specimens were imaged using high-resolution magnetic resonance imaging and magnetic resonance microscopy. Landmarks and volume data were collected and analysed. Findings demonstrated massive increases of brain size and eye size as well as flattening of the midline cranial base, facial projection and orbital margin frontation. Little evidence was found to support the notion that growth of the brain or nasal septum physically drives the observed changes of the skull. However, increases in the size of the eyes relative to skull size were associated with orbital margin frontation. With the possible exception of the results for eye size, the findings indicate that rather than forcing change the soft-tissues form a framework that physically constrains the morphogenetic template of the skeletal elements. This suggests, for example, that the degree of cranial base angulation seen in adulthood is not directly determined by brain expansion bending the basicranium, but by brain enlargement limiting the extent of cranial base flattening (retroflexion) in the fetus.
Key words basicranium; brain; convergence; development; evolution; frontation; orbits; primate; spatial-packing; tarsier.

Introduction

Studies of tarsier cranial anatomy have fuelled considerable debate in the past regarding the origins and taxonomic affinities of Tarsiiformes (e.g. Cartmill, 1974; Simons & Rasmussen, 1989; Ross, 1996; Ross et al. 1998; Ravosa & Savakova, 2004; Ross & Kay, 2004; Rossie et al. 2006). The three main competing hypotheses were that the tarsiers are most closely related to strepsirhines, that tarsiers are most closely related to the anthropoids or that tarsiers are independently derived (Szalay & Wilson, 1976; Beard et al. 1991; Ross, 1993; Ciochon & Gunnell, 2002; Bloch & Silcox, 2006). The balance of neontological, palaeontological and molecular evidence favours the link with the anthropoids. However, contention still persists as to the significance of the various cranial traits used to assign tarsiers to one or other group (see Kay et al. 1997; Schwartz, 2003; Rossie et al. 2006). Cranial traits commonly used include, for example, loss of the tapetum lucidum, possession of a fovea centralis, presence of an enlarged promontory branch of the internal carotid as well as the presence of a bony postorbital septum and reduced olfaction (see review in Miller et al. 2005). The question is, to what extent does, for example, the orbital morphology reflect shared phylogeny as opposed to morphological convergence due to the structural demands of accommodating the massive tarsier eyes (see Simons & Rasmussen, 1989)? Clearly insights into whether soft-tissues like the eyes can significantly alter skull architecture would be useful. Moreover, presumably such insights from a slightly

Correspondence
Dr Nathan Jeffery, Division of Human Anatomy & Cell Biology, School of Biomedical Sciences, University of Liverpool, Sherrington Building, Ashton Street, Liverpool L69 3GE, UK. T: +44 (0)151 7945514; F: +44 (0)151 7945517; E: njeffery@liverpool.ac.uk

Accepted for publication *22 February 2007*

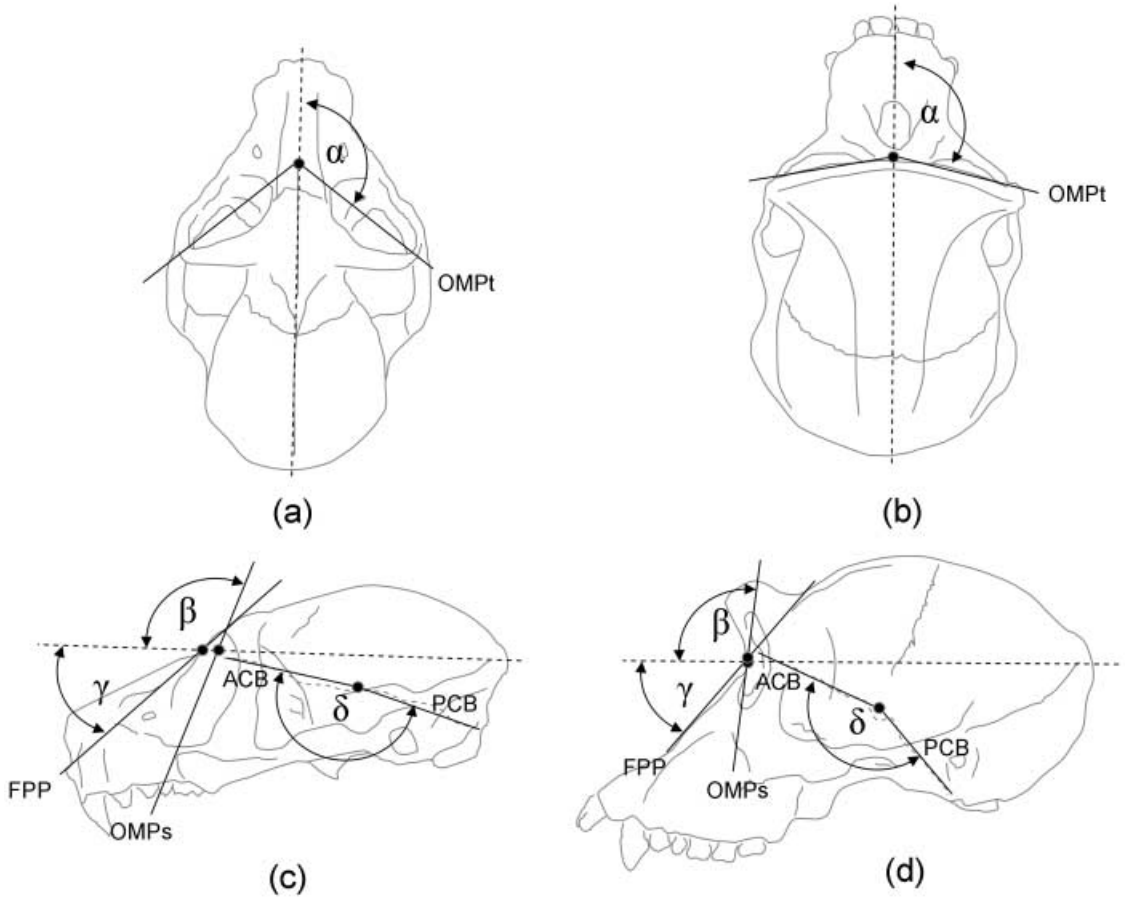

Fig. 1 Diagrams of a lemur (*Lemur catta*; a,c) and a chimp (*Pan troglodytes*; b,d) skull in superior (a,b) and lateral (c,d) profile illustrating measurements of convergence, frontation, midfacial prognathism and orbito-facial integration: MSP, midsagittal plane (broken line, a,b); OMPt, plane that passes through the medial- and lateral-most margins of the orbit and intersects with MSP; the angle of orbital convergence is equal to 180° – α; INP, plane from inion to nasion (broken line, c,d); OMPs, plane that passes through the superior- and inferior-most margins of the orbit and intersects with INP; the angle of orbital frontation is equal to 180° – β; FPP, midfacial prognathism plane through nasion and the anterior nasal spine; the angle of facial projection is equal to 180° – γ; ACB and PCB, planes marking the endocranial surfaces of the anterior cranial base and posterior cranial base, respectively; the angle of cranial base flexion is equal to δ. Not to scale.

different perspective, such as an ontogenetic study, would be particularly welcomed. The present study sets out to explore the most changeable part of tarsier ontogeny by documenting for the first time skull development in fetal specimens of *Tarsius bancanus*. The paper then tests hypotheses linking changes of bony skull morphology to the spatial requirements of the soft-tissues of the brain, the eyes and the cartilaginous nasal septum.

Over the last two centuries, numerous researchers have compared the crania of extant and extinct adult primates and perceived patterns in their morphological differences (Huxley, 1861; Dubois, 1869; Rutimeyer, 1871). The most noticeable, and thus most documented trends, include changes from a prosimian-like flat midline cranial base, prognathic face, and open and divergent orbits, to the highly flexed base, retrognathic face and encapsulated, forward-facing (frontated) and medially convergent orbits seen in great apes (Fig. 1) (Le Gros Clark, 1934; Cartmill, 1974, 1978; Ross, 1995). Several researchers have subsequently developed ideas that centre around the primacy of soft-tissue growth and evolution in the shaping of these skull features (Moss & Young, 1960; Moss, 1997a,b). In contrast to a purely reductionist view of morphological inheritance, proponents argue that it is not necessary, nor desirable, to preprogramme (i.e. genetically determine) each and every morphological detail. In many cases the physical environment, both internal and external, and interpreted in its widest sense, can be

relied upon to deliver an equitable outcome generation after generation whilst also allowing for rapid within-generation adaptation should that guiding environmental influence suddenly shift (Gould & Lewontin, 1979; Gould, 2002). With this in mind, it has been postulated in various and numerous ways that growth and evolution of the soft-tissues has helped shape the primate skull (e.g. Weidenreich, 1941; Biegert, 1963; Enlow & Hunter, 1968; Duterloo & Enlow, 1970; Enlow & McNamara, 1973). To exhaustively explore all of the proposals and their various permutations is impractical and would simply add to the morass. Nevertheless, common themes do emerge from the literature that warrant further investigation. These themes are referred to here as the spatial-packing hypotheses. In essence, these hypotheses suggest that in order to accommodate progressive phylogenetic, or ontogenetic, enlargement of the brain, eyes and of the cartilaginous nasal septum, the basicranium flexes and the orbits frontate and converge towards the midline. Convergence in turn reduces the amount of anterior facial projection that can be structurally supported by the interorbital region (Enlow, 1990). The overall effect is to maximize the space available for the soft-tissues by rearranging the major skeletal components, though of course the effects can be limited by more immediate functional constraints (e.g. the orbits cannot converge too closely without impinging on the function of vision).

The spatial packing hypotheses are supported by data from several comparative studies of extant adult primates and limited experimental work (e.g. Copray, 1986). With regard to the influence of the brain, Ross and colleagues' extensive comparative work documents a substantial degree of orbital convergence and frontation as well as flexion of the basicranium across extant adult primates (Ross & Ravosa, 1993; Ross, 1993, 1995). These changes were found to be strongly associated with large-scale increases of endocranial size relative to the length of the basicranium. This lends support to Gould's (1977) previous suggestion that the problem of packing in a larger brain is a major influence on the skull and basicranium in particular (see also Spoor, 1997; Noble et al. 2000; Ravosa et al. 2000; Barton, 2004; Ravosa & Savakova, 2004).

Comparative studies of eye and orbit size have also demonstrated links with changes of skull architecture (Schultz, 1940; Moss & Young, 1960; Enlow & McNamara, 1973; McCarthy & Lieberman, 2001). Cartmill (1974) originally proposed that orbital convergence is linked to increasing orbit size relative to skull size and that this relationship can be used to infer the nocturnal and diurnal habits of primates. While the link between relative orbit size and activity pattern in primates is supported (see Kay & Cartmill, 1977; Kay & Kirk, 2000; Heesy, 2004; Kirk, 2006), the proposed association of relative orbit size with convergence, and the potential knock-on effects of convergence on facial projection have not been fully explored. Some support for a link between eye size and changes of skull architecture can be found in the results from experiments on animals that involve enucleation and studies of human pathologies that influence the size of the eyes (Sarnat, 1978, 1982; Bukovic et al. 1997).

A third soft-tissue component contained within the fetal primate skull that may also influence the orientation of the orbits, face and cranial base is the midline cartilaginous lamina that extends from the crista-galli and vomer to the anterior border of the presphenoid. In the primate fetus the lamina is one cartilaginous structure flanked by the paraseptal cartilages and continuous with the mesethmoid (De Beer, 1985; Lozanoff et al. 2004). In adults the mesethmoid part ossifies and extends to form the perpendicular plate of the ethmoid whilst the rostral part remains cartilaginous as the nasal septum. For convenience we refer to the larger, continuous structure seen in the fetus as the cartilaginous nasal septum (see Fig. 3), although strictly speaking this term refers only to the part that remains cartilaginous in adulthood (Sperber, 1981). Once considered by Scott (1953) to be a major expansive force in shaping the face, the cartilaginous nasal septum is now believed by many to play more of a passive role (Moss et al. 1968; Carlson, 1985; Enlow, 1990). Indeed, *ex-vivo* experimental data indicate that the septum is primarily morphogenetic (Koski, 1968; Ronning & Kantomaa, 1985). However, Enlow (1990) contests that there can be no genetic blueprint for the nasal septum. Irrespective of the nature of formation and the role played in the skull, the septum is clearly an important component. This is substantiated by numerous animal experiments, investigations of developmental abnormalities and reports of surgical interventions as well as studies of ontogenetic and adult comparative samples (e.g. Schultz, 1935; Scott, 1953, 1958; Ford, 1956; Moss et al. 1968; Glanville, 1969; Kvinnsland, 1970, 1974; Verwoerd et al. 1979, 1980; Copray, 1986; Adamopoulos et al. 1994; Hans et al. 1996; Jeffery, 1999; Jeffery & Spoor, 2004; Bastir & Rosas, 2005). These all report major

changes of skull architecture associated with alterations to the size and or shape of the nasal septum. The above spatial-packing hypotheses can be summarized as follows:

Brain hypothesis. This hypothesis states that changes in the position of the orbits, facial orientation and angulation of the midline basicranium are the structural consequences of fitting in a rapidly enlarging brain along a slower growing basicranium (for details of the original hypothesis see Ross & Ravosa, 1993). The hypothesis predicts that orbital convergence and frontation, a reduction of facial projection as well as a reduction in the ventral angle between the posterior and anterior components of the basicranium (cranial base angle) are significantly correlated with increases in the size of the brain relative to the length of the skull base. However, the endocranium is not an amorphous volume. It is structurally divided by the tentorium cerebelli into infratentorial and supratentorial parts (Jeffery, 2002). Therefore, two corollary hypotheses with the supratentorial brain relative to the anterior base and the infratentorial brain relative to the posterior base will also be tested.

Eye hypothesis. This hypothesis is derived from ideas first proposed by Cartmill (1974) and states that changes of orbital convergence and frontation, facial orientation and angulation of the midline basicranium are the structural consequences of accommodating rapidly enlarging eyes within a slower growing skull. The hypothesis predicts that increases of eye size relative to skull size are significantly correlated with orbit convergence, orbit frontation and cranial base flexion as well as reduction of facial projection.

Brain and eye hypothesis. This hypothesis is a modified version of the brain–basicranium and eye–skull hypotheses (see above) and incorporates the additional structural demands of accommodating both enlargement of the eyes and brain. The hypothesis predicts that orbit convergence, orbit frontation and cranial base flexion as well as a reduction of facial projection are significantly correlated with the combined increases of the endocranium and eyes (1) relative to skull size and (2) relative to cranial base length.

Nasal septum hypothesis. The cartilaginous nasal septum separates the orbits and supports the face and the anterior cranial base. It therefore seems pertinent to explore the potential impact of the septum as Scott had originally intended, that is as a spatial packing force within the skull. We are not aware of any previous studies of relative nasal septum size. Consequently, it is not clear which skull element(s) should be used to make relative measurements of the septum. Here we have taken the two most common denominators of cranial base length and skull size as well as a third spatially linked denominator of anterior cranial base length (Jeffery & Spoor, 2004). The hypothesis predicts that orbit convergence, orbit frontation and cranial base flexion as well as a reduction of facial projection are significantly correlated with increases of nasal septal area relative to (1) skull volume, (2) cranial base length and (3) anterior cranial base length.

Combined soft-tissue hypothesis. The final hypothesis is a synthesis of the above hypotheses and proposes that the problem of packing in enlargement of the nasal septum, eyes and brain drives orbital convergence, frontation as well as cranial base flexion and a reduction of facial projection. Again, it is not clear which denominator is the most appropriate. Hence, the hypothesis predicts that angular changes of the basicranium, orbits and facial projection are correlated with combined increases of brain size, eye size and septum size relative to (1) skull size and (2) cranial base length.

To accept any of the above hypothesis, the results must reveal significant correlations of increases in relative sizes with increases of base flexion, orbital convergence and orbital frontation as well as with decreases of facial prognathism. As such, the hypotheses are formulated to focus on identifying only the principal factors shaping the developing tarsier skull. If the findings fail to demonstrate the correlations predicted then the hypothesis will be considered falsified. However, it is important to note that the hypothesis can only be considered falsified within the terms of the present study. For instance, it is possible that any one of the above scenarios partly explains the changes, but will be falsified here because it does not explain the bulk of the changes. Also, factors playing only a minor role in shaping the fetal skull, and therefore rejected here, may come to play more prominent roles later in development. Finally, additional and alternative factors not identified here may also contribute to the processes and mechanisms shaping the fetal tarsier skull. Notwithstanding these caveats, the testing of the above spatial-packing hypotheses should yield

Table 1 Sample details and raw data (see Table 2 for measurement details)

ID	MQ%	Skull volume (mm^3)	Brain volume (mm^3)	Infra-tentorial volume (mm^3)	Total eye volume (mm^3)	Septal area (mm^2)	Base length (mm)	Posterior base length (mm)	AOMc (°)	AOAc (°)	AOMf (°)	AOAf (°)	AFP (°)	CBA (°)
528	26	336	126	62	17	3	6.0	3.4	127	43	128	15	67	161
602	27	432	279	94	39	4	7.1	3.4	127	45	122	23	70	158
661	38	924	447	120	106	7	8.4	3.6	131	37	122	21	82	152
471	40	1152	425	107	166	8	9.4	3.9	122	37	119	14	76	161
739	41	1573	481	125	161	7	9.3	4.2	116	32	117	21	74	162
351	43	1872	581	144	165	8	9.9	4.3	126	41	128	13	71	151
352	46	1755	667	157	263	10	11.1	5.1	132	38	122	23	71	165
103	47	2250	747	191	348	9	11.3	5.2	120	37	120	24	83	156
76	53	1512	675	185	356	10	10.9	4.9	127	42	120	34	74	163
554	59	3366	1519	213	846	15	13.6	5.6	120	42	107	22	81	162
782	63	2970	1352	199	890	20	13.5	5.5	127	37	105	15	79	163
509	68	3744	1428	213	991	17	13.7	5.6	126	43	101	21	85	160
910	73	3648	1436	280	866	15	13.8	5.7	132	41	110	22	87	165
495	74	3468	1788	236	782	17	13.2	5.5	105	40	95	16	84	161
955	75	3876	1874	251	1026	19	14.1	5.5	127	38	114	16	81	164
781	78	3840	1539	209	1042	18	13.7	5.6	121	37	106	20	79	166
281	81	4284	1759	230	990	18	14.0	5.6	128	43	117	25	80	162
405	81	4641	1951	284	850	17	15.5	6.3	126	25	112	23	75	157
407	100	5796	2374	321	1603	30	16.5	6.6	124	35	109	13	85	167

important insights into the major factors shaping development of the fetal tarsier skull.

Methods and materials

The sample consists of 19 post-mortem fetal *T. bancanus* specimens from the Hubrecht Laboratorium, the Netherlands (Richardson & Narraway, 1999). Details are given in Table 1. Measurements of crown–rump length (CRL; Streeter, 1920) were recorded for each specimen and ranged from 16.1 to 62.4 mm CRL. Wharton (1950) reports that a newborn captive bred *Tarsius cabonarius* (syn. *T. syrichta*) had a body length of 60 mm. Adult body masses for *T. syrichta* (117–134 g) are similar to *T. bancanus* (111–120 g). Thus, we assumed here that the largest specimen (62.4 mm) in the present sample is perinatal. To aid comparison between individuals and with previous fetal studies (Jeffery, 2003; Jeffery & Spoor, 2006) a quotient of maturation (MQ) was calculated as the percentage of CRL at birth (16.1–62.4 mm; 26–100% MQ). The sample covers the last three-quarters of the gestational life history of *T. bancanus*.

Fetuses were imaged either with a horizontal 7-Tesla Magnex magnet (Abingdon, Oxfordshire, UK) interfaced to an SMIS/MRSS console (Guildford, Surrey, UK), Imaging Science and Biomedical Engineering, University of Manchester, or with a vertical 9.4-Tesla Bruker (Rheinstetten, Germany) microimaging system, Sir Peter Mansfield Magnetic Resonance Centre, University of Nottingham. In both cases, multislice spin-echo images were acquired with slices thickness from 0.15 to 0.32 mm (dependent on the size of the fetus). Imaging parameters for the Magnex system were TR = 6 s, TE = 55 ms and 46 averages. Those for the Bruker system were TR = 7 s, TE = 35 ms and 60 averages. After acquisition the data were zero-filled to 256×256 or 512×512 data points, Fourier transformed and exported as raw binary files. Images were then interpolated using the ImageJ software (W. Rasband, NIH of Mental Health, Bethesda, MD, USA) and the TransformJ bicubic spline function (Meijering et al. 2001) to form isotropic voxels with vertices ranging from 0.05 to 0.10 mm.

The craniofacial region was defined by a set of landmarks given in Table 2. Three-dimensional coordinates for each landmark were acquired from isotropic data sets using ImageJ (rsb.info.nih.gov/ij/) and then used to define line segments. Lines were measured against midsagittal (MSP) and lateral canal (LSCP) reference lines to obtain the angles of orientation detailed in Table 2. Numerous alternative references lines and planes have been used in the past including, for example, the Frankfurt Horizontal or the inion to nasion plane

Table 2 Landmarks, lines and measurements

Measurement	Notation	Description
Landmarks		
Orbital inferior	Oi	point of orbital margin closest to the toothrow
Orbital superior	Os	point of the orbital margin furthest from the toothrow
Orbital medial	Om	point on the orbital margin closest to the junction between the frontonasal and internasal sutures
Orbital lateral	Ol	point on the orbital margin furthest from the junction between the frontonasal and internasal sutures
Optic canal	Oc	point marking the centre of the opening of the optic canal into the orbit
Anterior lateral canal	LSCa	centre of lumen of the anterior limb of the lateral canal at its widest point
Posterior lateral canal	LSCp	centre of lumen of the posterior limb of the lateral canal at its widest point
Basion	Ba	The midline point on the anterior margin of the foramen magnum
Foramen caecum	Fc	The midline point marking the pit between the fetal crista galli and the endocranial wall of the frontal bone
Pituitary point	Pp	The midline point on the raised tuberculum sella of the body of the sphenoid.
Anterior nasal margin	ANM	The midline point marking the intersect between the rostral most tip of the nasal septum and the surface of the maxilla
Posterior nasal spine	PNS	The midline point on the tip of the posterior nasal spine
Hormion	H	The posterior-most midline point on the junction between the ventral surface of the sphenoid and the vomeral root
Pterygomaxillare	Ptm	the junction between the medial and lateral pteryoids and maxilla
Lines		
Midsagittal line	MSP	Line passing through Fc, Pp and Ba and projected onto the transverse plane of the skull
Lateral canal line	LCP	Line passing through the anterior and posterior limbs of the lateral semicircular canal (LSCa-LSCp) and projected onto the sagittal plane of the skull
Angles (°)		
Angle of orbital margin convergence	AOMc	Angle of a line passing through the medial most (Om) and lateral-most (Ol) margins of the orbit against the midsagittal plane
Angle of orbital axis convergence	AOAc	Angle of a line passing through the centroid of all orbital margin landmarks (Os, Oi, Ol and Om) and the optic canal (OC) against the midsagittal plane
Angle of orbital margin frontation	AOMf	Angle of a line passing through the inferior-most (Oi) and superior-most (Os) margins of the orbit against the lateral canal plane
Angle of orbital axis frontation	AOAf	Angle of a line passing through the centroid of all orbital margin landmarks (Os, Oi, Ol and Om) and the optic canal (OC) against the lateral canal plane
Angle of facial projection	AFP	Angle of a line passing through the foramen caecum (Fc) and the anterior nasal margin (ANM) against the lateral canal plane
Cranial base angle	CBA	Angle between lines passing through foramen caecum (Fc), pituitary point (Pp) and basion (Ba)
Lengths, areas and volumes		
Skull height	Sh	Maximum distance in the midline from the base of the basisphenoid to the top of the cranial vault
Skull width	Sw	Distance marking the widest distance in the axial plane.
Skull length	Sl	Maximum distance in the midline from nasion to opisthocranion
Cranial base length (mm)	TBL	Total distance from foramen caecum (Fc) to pituitary point (Pp) to basion (Ba)
Anterior base length (mm)	ABL	Distance from foramen caecum (Fc) to pituitary point (Pp)
Posterior base length (mm)	PBL	Distance from pituitary point (Pp) to basion (Ba)
Skull volume (mm^3)	SKV	Multiple of skull height, width and length
Nasal septum area (mm^2)	NSA	Area of the cartilaginous mesethmoid (nasal septum plus perpendicular plate of ethmoid) taken from the midsagittal slice.
Eye ball volume (mm^3)	EBV	Summated outlined areas of both eyeballs taken in transverse slices
Endocranial volume (mm^3)	EV	Summated outlined areas of the endocranial cavity taken in sagittal slices
Supratentorial volume (mm^3)	SV	Summated outlined areas of the endocranial cavity above the tentorium cerebelli taken in sagittal slices
Infratentorial volume (mm^3)	IV	Summated outlined areas of the endocranial cavity below the tentorium cerebelli taken in sagittal slices

Table 2 *Continued*

Measurement	Notation	Description
Relative sizes		
Index of relative endocranial volume	IRE	Cube root of endocranial volume (EV) divided by the length of the cranial base (TBL)
Index of relative supratentorial volume	RSE	Cube root of the supratentorial volume (SV) divided by the length of the anterior cranial base (ABL)
Index of relative infratentorial volume	RIE	Cube root of the infratentorial volume (IV) divided by the length of the posterior cranial base (PBL)
Index of relative eye volume	IRO	Eye volume (EBV) divided by skull volume (SKV)
Index of relative endocranial and eye volume i	IREOi	Cube root of eye (EBV) plus cube root endocranial volume (EV) divided by cube root skull volume (SKV)
Index of relative endocranial and eye volume ii	IREOii	Cube root of eye (EBV) plus cube root endocranial volume (EV) divided by cranial base length (TBL)
Index of relative nasal septal size I	IRNi	Square root of nasal septum area (NSA) divided by cube root skull volume (SKV)
Index of relative nasal septal size ii	IRNii	Square root of nasal septum area (NSA) divided by cranial base length (TBL)
Index of relative nasal septal size iii	IRNiii	Square root of nasal septum area (NSA) divided by anterior cranial base length (ABL)
Index of relative soft-tissue size I	IRSTi	cube root of endocranial volume (EC) plus cube root of eye volume (EBV) plus sqaure root of septum area (NSA) divided by cube root skull volume (SKV)
Index of relative soft-tissue size ii	IRSTii	cube root of endocranial volume (EC) plus cube root of eye volume (EBV) plus sqaure root of septum area (NSA) divided by cranial base length (TBL)

(INP). A critical problem with all reference lines is the potential for bias caused by changes in their orientation, leading to false positive correlations between angles measured against the reference. Datum point coordinates were therefore analysed a second time with non-Euclidian methods of geometric morphometrics that allow for the exploration of shape changes within a landmark suite without reference to any one line. The implementation employed here was Morphologika™, developed by O'Higgins and colleagues, University College London (O'Higgins & Jones, 1998; O'Higgins, 2000a,b). The software employs a generalized least-squared Procrustes superimposition to remove scaling, translation and rotation between landmark forms. This leaves residual shape information in the form of Procrustes coordinates for each specimen within a complex multidimensional shape-space. The ten major axes of shape variation within this space were explored with principal components analysis (PCA). For full technical details see O'Higgins & Jones (1998).

The angle of orbital convergence was measured in two ways. First, as the anterior angle between the MSP and a line passing through the medial (Om) and lateral (Ol) most margins of the orbit. This angle is referred to as the angle of orbital margin convergence (AOMc). A second anterior angle was taken between MSP and a line referred to as the orbital axis plane (OAP), which passes through the centroid of all four orbit marginal landmarks (Oi, Os, Om and Ol) and through the optic canal (Oc). This angle, called the angle of orbital axis convergence (AOAc), provides additional information on convergence. The angle of orbital frontation was also measured in two ways. The first angle, called the angle of orbital margin frontation (AOMf), was taken as the anterosuperior angle between the line of the lateral canal (LSCa-LSCp) and a line through the inferior- (Oi) and superior- (Os) most margins of the orbit. The second angle taken, called the angle of orbital axis frontation (AOAf), was taken between OAP and the plane of the lateral canal. In order to investigate the proposed effects of convergence on the face, an angle of facial projection (AFp) was taken between the line of the lateral canal and a line through foramen caecum (Fc) and the anterior nasal margin (ANM). The angle of cranial base angulation (CBA) was taken between Fc, pituitary point (Pp) and basion (Ba). Additional landmarks were taken to help resolve any shape changes of the orbits and surrounding face. These were the posterior nasal spine (PNS), hormion (H) and pterygomaxillare (Ptm). Because the landmarks are type II (e.g.

orbital margins) as well as type I (e.g. foramen caecum) we can expect see some shape variance due to random landmarking error of the less homologous type II landmarks (Bookstein, 1992). However, because the errors are random they are unlikely to obscure the analyses provided steps are taken to identify and describe only those components of the shape space that are significantly associated with growth (MQ) or the spatial-packing variables.

Cranial base lengths were defined by the landmarks Fc, Pp and Ba. Landmarks and angles are demonstrated on Figs 2–4 and described in Table 2. The area of the nasal septum was taken by hand from midsagittal scans using the ImageJ trace facility (see Fig. 3). The inferior (ventral) margin of the septum was defined by the border with the vomer. The posterior margin was defined by the border with the presphenoid and the superior border runs under the mesethmoid in the interorbital region. Measurements of endocranial, supratentorial and infratentorial as well as eye volume were computed by outlining by hand (ImageJ trace facility) the margins of these structures in each slice and summing the area measurements. These data were used to compute values of relative endocranial sizes, relative eye sizes and relative septum sizes given in Table 2. A previous study by one of us (N.J.) used similar samples and methods and showed that the measurement errors incurred are insignificant comparison with the biological variation (Jeffery & Spoor, 2002).

Associations between bivariate measurements and shape data were analysed with Spearman's rank correlations and Reduced Major Axes regressions in PAST (http://folk.uio.no/ohammer/past). A potential problem with studying such a changeable period of ontogeny is that structurally independent measurements that strongly correlate with fetal size (or age) can also appear to be correlated with each other as their independent variations are carried along together by the same massive growth changes (Jeffery & Spoor, 2004). A somewhat simplistic analogy is of two people running in opposite directions on a speeding train. To an observer on the track side both people appear to be

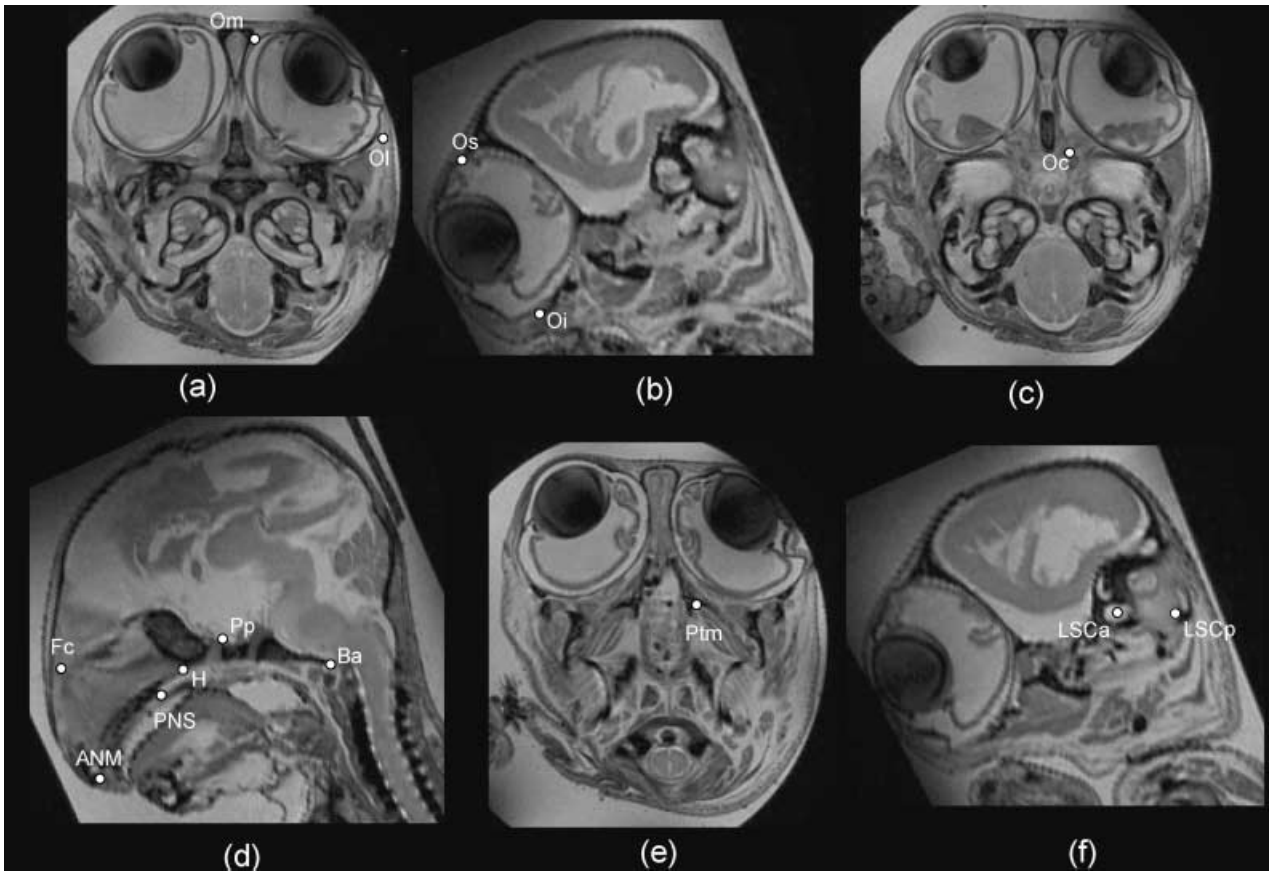

Fig. 2 Sagittal (b,d,f) and transverse (a,c,e) high-resolution MR scans illustrating the landmarks used (Specimen 781, crown–rump length = 48.6 mm; see Table 2 for abbreviations).

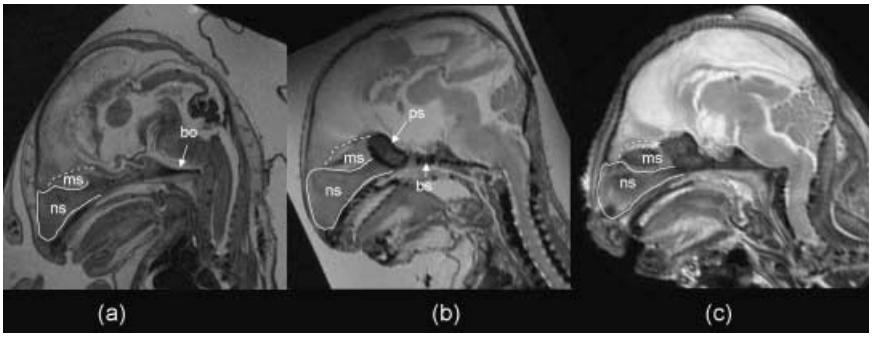

Fig. 3 Midline MR images of the fetal tarsier skull at (a) 29.2 mm, (b) 48.6 mm and (c) 62.4 mm crown–rump length. These illustrate that the basicranium gradually ossifies from basioccipital (bo), basisphenoid (bs) and presphenoid (ps) centres and that the mesethmoid (ms) also gradually ossifies and is continuous with the nasal septum (ns). Not to scale.

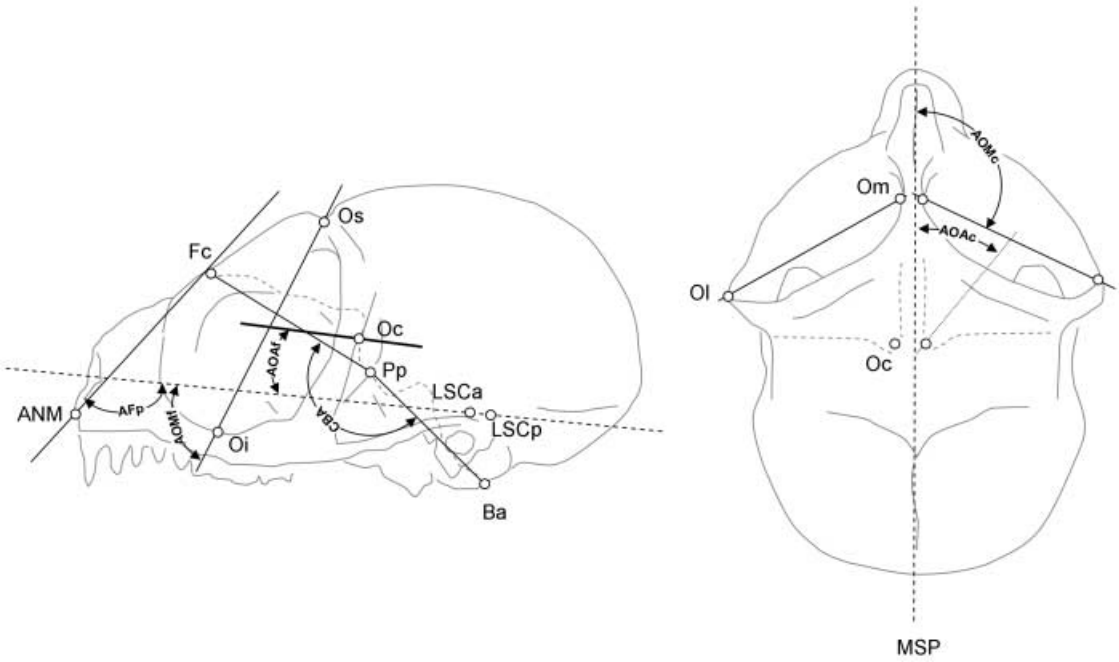

Fig. 4 Sketches showing lateral (left) and superior (right) views of a tarsier skull and illustrating the landmarks and angles used (refer to Table 2 for details).

moving in the same direction albeit at different speeds. These false positive results are not always obvious and must be controlled for by conservative means. To minimize the compounding effects of growth (i.e. to stop the train!), partial correlations were computed with SPSS (v.12) whilst controlling for MQ. Similarly, regression analyses were conducted with the residuals of plots against MQ. Correlations that remain significant after these stringent criteria have been applied will be considered reliable indicators of possible spatial-packing interactions. Slopes were compared with standard *F*-tests. Statistics with probability values less than 0.05 were deemed significant.

Results

Raw measurements for each fetus are presented in Table 1. A basic understanding of the growth-related trends evident within the sample is required to contextualize the hypotheses testing. Plots of angles, lengths, areas and volumes as well as relative sizes were made against the maturation quotient (MQ). Statistics for each of these plots are presented in Table 3. Bivariate comparisons reveal that the angle of orbital margin frontation (AOMf) decreases significantly as the fetus matures whereas the angle of facial projection (AFP) and cranial base angle (CBA) increase significantly

Table 3 Bivariate comparisons against maturation quotient (MQ%)

vs. MQ	*R*-rank	*P*	*a*	95% CI *a*	*b*
AOMc	–0.10	ns			
AOAc	–0.23	ns			
AOMf	–0.70	***	–0.438	–0.632 > –0.289	140.100
AOAf	0.05	ns			
AFP	0.56	*	0.282	0.219 > 0.369	61.566
CBA	0.47	*	0.212	0.125 > 0.311	148.390
TBL	0.96	***	0.140	0.119 > 0.161	3.635
ABL	0.97	***	0.095	0.081 > 0.113	1.244
PBL	0.92	***	0.046	0.039 > 0.054	2.309
$SKV^{1/3}$	0.97	***	0.150	0.124 > 0.175	4.529
$EV^{1/3}$	0.97	***	0.115	0.098 > 0.135	3.165
$IV^{1/3}$	0.94	***	0.037	0.030 > 0.045	3.486
$SV^{1/3}$	0.96	***	0.120	0.102 > 0.143	2.173
$EBV^{1/3}$	0.92	***	0.128	0.110 > 0.149	0.236
$NSA^{1/2}$	0.92	***	0.046	0.040 > 0.052	0.796
IRE	–0.05	ns			
RSE	–0.40	ns			
RIE	–0.75	***	–0.005	–0.006 > –0.003	1.411
IRO	0.77	***	0.004	0.003 > 0.005	–0.030
IREOi	0.67	**	0.005	0.003 > 0.007	1.008
IREOii	0.70	***	0.005	0.003 > 0.006	1.208
IRNi	0.28	ns			
IRNii	0.34	ns			
IRNiii	–0.38	ns			
IRSTi	0.67	**	0.006	0.004 > 0.008	1.222
IRSTii	0.68	**	0.005	0.004 > 0.007	1.471

*$P < 0.05$; **$P < 0.01$; ***$P < 0.001$; ns, not significant.

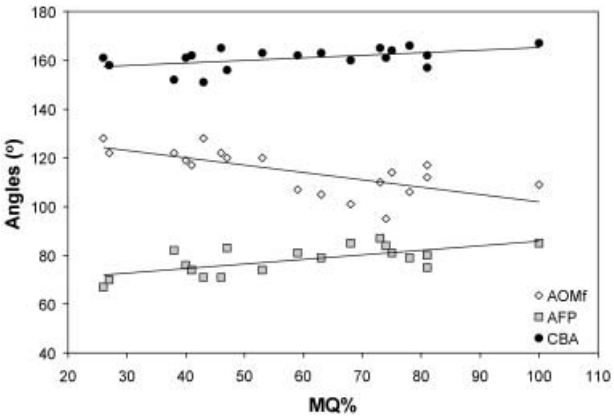

Fig. 5 Plots of angle of orbital margin frontation (AOMf), angle of facial projection (AFP) and cranial base angle (CBA) against the maturation quotient (MQ). Reduced major axes regressions shown.

(Fig. 5). The remaining angles show no significant correlations with MQ. These results reveal that as the fetus matures the orbits tilt up to lie more perpendicular relative to the lateral semicircular canal (LSC), the face

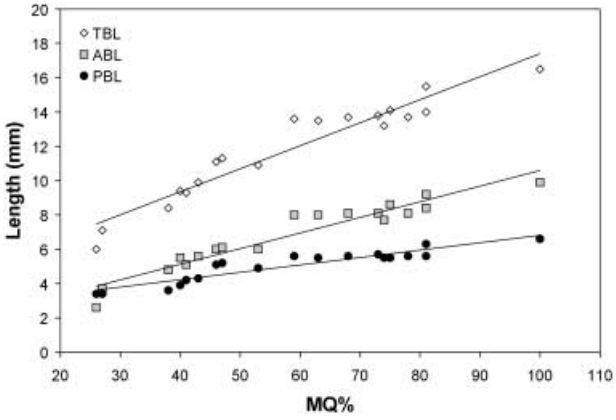

Fig. 6 Plots of total cranial base length (TBL), anterior base length (ABL) and posterior base length (PBL) against the maturation quotient (MQ). Reduced major axes regressions shown.

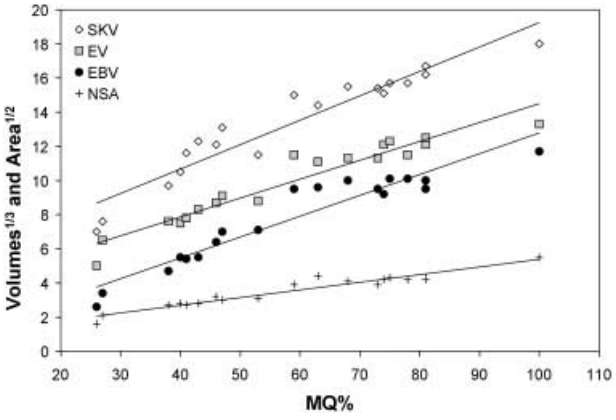

Fig. 7 Plot of cube root skull size (SKV), square root nasal septum area (NSA), cube root endocranial volume (EV) and cube root total eye volume (EBV) against the maturation quotient (MQ). Reduced major axes regressions shown.

tips further forward and the cranial base flattens out slightly. Correlations computed to determine if there is any structural integration of AOMf and AFP with CBA were insignificant (r_{rank} = –0.38 ns, 0.18 ns, respectively).

Not surprisingly, increases in length, area and volume showed highly significant positive correlations with fetal maturation (Table 3; Figs 6 and 7). The slope for the anterior base shown in Fig. 6 is significantly greater than that for the posterior base ($P < 0.001$). Figure 7 demonstrates plots of skull volume (SKV), endocranial volume (EV), combined eye volume (EBV) and nasal septum area (NSA) against MQ. Plots for infratentorial and supratentorial volume are not shown but details are given in Table 3. All plots are made dimensionally

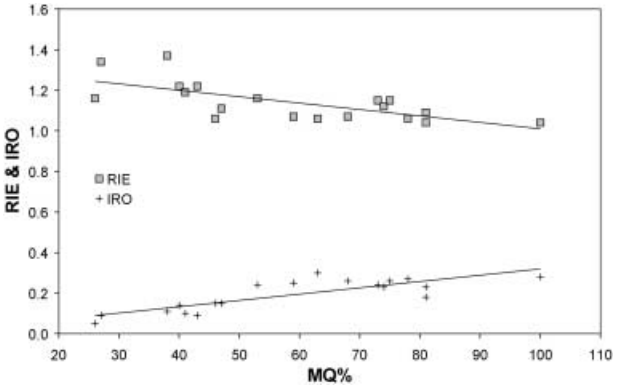

Fig. 8 Plot of relative infratentorial size (RIE) and relative eye size (IRO) against the maturation quotient (MQ). Reduced major axes regressions shown.

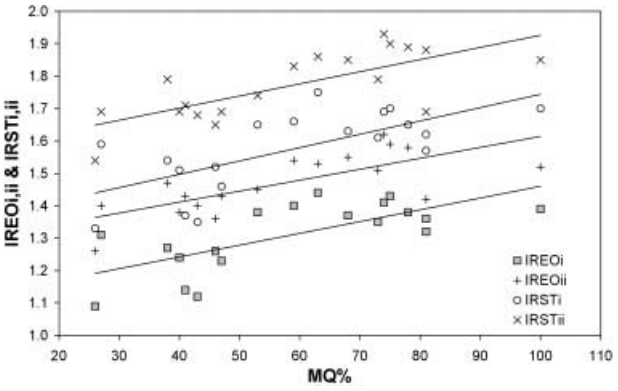

Fig. 9 Plots of eye plus brain size relative to skull size (IREOi) and relative to cranial base length (IREOii) and plots of combined soft tissues relative to skull size (IRSTi) and relative to cranial base length (IRSTii). Reduced major axes regressions shown.

equivalent to the MQ variable using cube and square roots. The slope for combined eye volume is significantly greater than that for endocranial volume ($P < 0.05$).

To determine if any of the potential spatial packing problems worsen as the fetus matures, plots of relative endocranial, eye and nasal septal sizes were made against MQ. There were no significant changes in relation to MQ for endocranial size relative to base length (IRE), supratentorial size relative to anterior base length (RSE) or relative nasal septum size (IRNi, ii, iii). Details of significant changes of spatial packing variables against MQ are given in Table 3. Plots of infratentorial size relative to posterior cranial base length (RIE) reveal a significant decrease (Fig. 8). This shows that as the fetus matures the proposed problem of squeezing in a larger infratentorial brain along the posterior cranial base actually diminishes slightly. By contrast, the size of the eyes relative to skull size (IRO) does show a small but significant increase with fetal maturity. This suggests that the proposed problem of packing in the large tarsier eyes within the skull gradually worsens as the fetus matures. The growth of the eyes also leads to significant growth-related increases of relative endocranial plus eye size (IREOi,ii) and relative soft-tissue size (IRSTi,ii) (see Fig. 9).

Plots of scores from principal components 1–10 were made against MQ to document fetal growth-related non-Euclidean shape changes. Only scores from the first PC (representing 32.3% of the total variance) were significantly correlated with MQ (Fig. 10; see Tables 6 and 7). The other nine components reveal low correlation coefficients in the range –0.07 to 0.27 (ns). Figure 10 shows the plot of PC1 vs. MQ with wireframe reconstructions from lateral and dorsal views of the mean shape at either end of the MQ range. Reconstructions show a flattening of the cranial base, a rotation of the orbits from facing slightly downward to facing forward, and a downward mediolateral bending of the palate as well as an anterior projection of the face. These changes are accompanied by relative decreases in the proportions of the nasal septum, basisphenoid region and basioccipital, together with relative increases in the proportions of the orbit.

Having established the general growth-related trends, the hypotheses were tested. Tests were carried out by comparing both angular measurements and PC scores against spatial-packing variables (Tables 4 and 6). In terms of the measurements taken, the spatial-packing hypothesis predicts that increases of relative size are negatively correlated with (1) the cranial base angle (representing basicranial flexion), (2) the angle of facial projection (representing a reduction of facial prognathism), (3) the angles of orbital axes convergence and frontation, and (4) the angle of orbital margin convergence. By contrast, the hypothesis predicts positive correlations with the angle of orbital margin frontation.

Significant correlations were observed with regard to the angle of orbital margin frontation (AOMf), angle of facial projection (AFP) and cranial base angle (CBA). These were correlated with several of the spatial-packing variables (RIE, IRO, IREOi,ii, IRNi, IRNii, IRSTi,ii). However, all of these measurements also show strong growth-related trends with regard to MQ (see

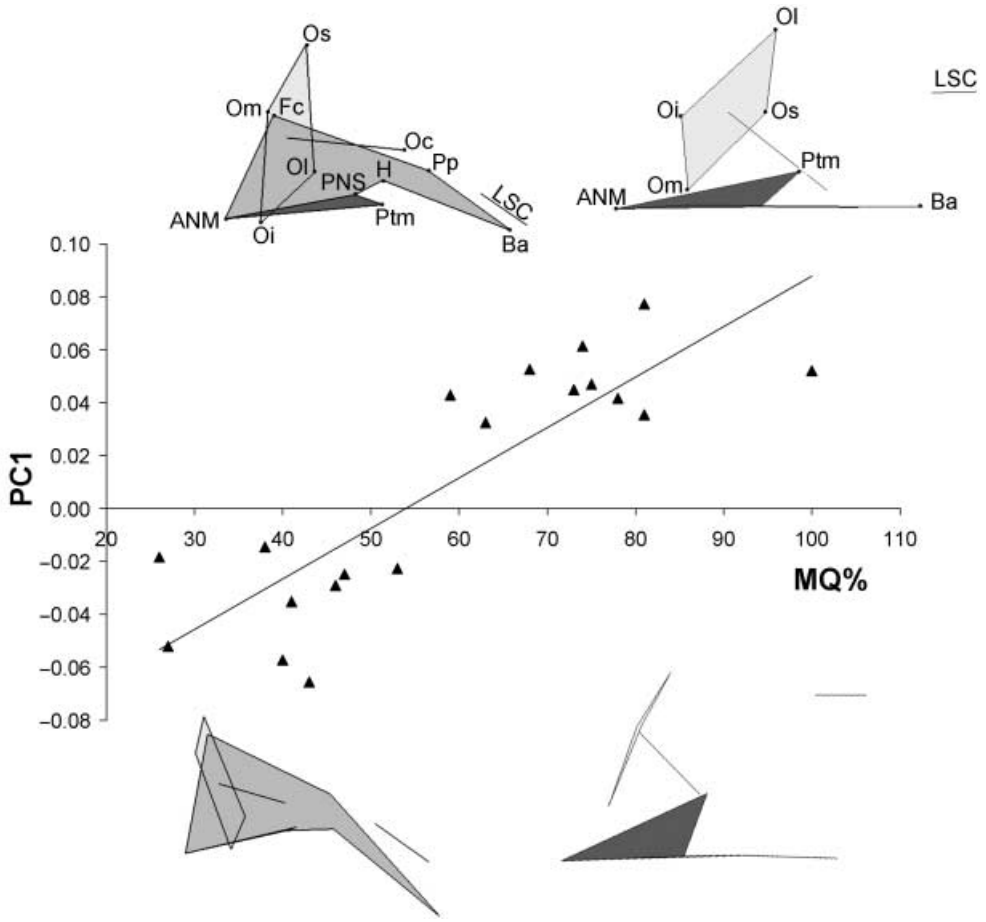

Fig. 10 Plot of principal component 1 (PC1) scores against the maturation quotient (MQ). Wireframe reconstructions from the lateral and dorsal view that illustrate shape changes across the MQ range are shown (refer to Table 2 for landmark details and see main text for a description of shape changes). Reduced major axes regression are also shown.

Table 4 Rank correlation matrix of spatial-packing measurements against angular measurements with partial correlations whilst holding MQ constant given in parentheses

	AOMc	AOAc	AOMf	AOAf	AFP	CBA
IRE	–0.03 ns	0.36 ns	–0.04 ns	–0.14 ns	0.02 ns	–0.25 ns
RSE	–0.04 ns	0.41 ns	0.27 ns	0.04 ns	–0.27 ns	–0.31 ns
RIE	0.12 ns	0.29 ns	0.61** (0.13 ns)	–0.06 ns	–0.31 ns	**–0.48*** (–0.37 ns)
IRO	–0.07 ns	–0.15 ns	**–0.80*** (–0.52*)**	–0.07 ns	**0.59**** (0.33 ns)	**0.64**** (0.40 ns)
IREOi	–0.06 ns	–0.01 ns	**–0.78*** (–0.51*)**	–0.05 ns	**0.51*** (0.30 ns)	**0.52*** (0.22 ns)
IREOii	–0.21 ns	0.03 ns	**–0.78*** (–0.59*)**	–0.03 ns	**0.68**** **(0.56*)**	0.34 ns
IRNi	0.08 ns	–0.13 ns	–0.43 ns	–0.29 ns	0.23 ns	**0.49*** (†)
IRNii	–0.03 ns	–0.19 ns	**–0.51*** (†)	–0.41 ns	0.43 ns	0.34 ns
IRNiii	0.16 ns	0.06 ns	0.22 ns	–0.31 ns	–0.32 ns	0.07 ns
IRSTi	–0.05 ns	0.01 ns	**–0.76*** (–0.49*)**	–0.08 ns	**0.51*** (0.26 ns)	**0.55*** (0.25 ns)
IRSTii	–0.17 ns	–0.04 ns	**–0.77*** (–0.57*)**	–0.11 ns	**0.64**** **(0.53*)**	0.40 ns

Significant correlations highlighted in bold type: *$P < 0.05$; **$P < 0.01$; ***$P < 0.001$; ns, not significant.
†IRNi,ii does not significantly correlate with MQ so partial correlation method invalid.

Table 5 Bivariate comparisons of residuals from plots against MQ for significantly correlated variables (see Table 4)

	R rank	*P*	*a*	95% *a*	*b*
AOMf residual vs. RIE residual	0.30	ns			
AOMf residual vs. IRO residual	–0.51	*	–156.38	–241.90 > –106.80	0
AOMf residual vs. IREOi residual	–0.54	*	–87.66	–125.40 > 62.70	0
AOMf residual vs. IREOii residual	–0.64	**	–105.88	–177.40 > –75.72	0
AOMf residual vs. IRNii†	–0.08	ns			
AOMf residual vs. IRSTi residual	–0.55	*	–72.80	–108.01 > –49.72	0
AOMf residual vs. IRSTii residual	–0.69	***	–92.35	–152.50 > –62.81	0
AFP residual vs. IRO residual	0.38	ns			
AFP residual vs. IREOi residual	0.43	ns			
AFP residual vs. IREOii residual	0.54	*	70.77	47.72 > 108.70	0
AFP residual vs. IRSTi residual	0.41	ns			
AFP residual vs. IRSTii residual	0.51	*	61.73	42.23 > 88.94	0
CBA residual vs. RIE residual	–0.50	*	–58.74	–83.79 > –40.21	0
CBA residual vs. IRO residual	0.46	*	96.53	61.67 > 151.40	0
CBA residual vs. IREOi residual	0.31	ns			
CBA residual vs. IREOii residual	0.07	Ns			
CBA residual vs. IRNi†	0.01	ns			
CBA residual vs. IRSTi residual	0.35	ns			

*$P < 0.05$; **$P < 0.01$; ***$P < 0.001$; ns, not significant.
†IRNi,ii does not significantly correlate with MQ so raw values were used.

Table 6 Rank correlation matrix for comparisons of maturation quotient and spatial-packing variables against the first ten principal components (PC) of shape space. Partial correlations whilst holding MQ constant given in parentheses for PC1 scores only

	PC1	PC2	PC3	PC4	PC5	PC6	PC7	PC8	PC9	PC10
Proportion of total variance (%)	32.3	18.7	12	10.1	7.6	3.7	3.4	2.7	2.2	1.9
MQ	**0.78*** **	0.11 ns	0.18 ns	0.27 ns	0.13 ns	–0.15 ns	–0.07 ns	0.03 ns	0.22 ns	0.11 ns
IRE	0.15 ns	0.38 ns	–0.21 ns	0.01 ns	–0.09 ns	–0.04 ns	–0.19 ns	0.16 ns	**–0.48***	–0.11 ns
RSE	–0.15 ns	0.39 ns	–0.15 ns	–0.06 ns	–0.19 ns	–0.02 ns	–0.01 ns	0.19 ns	–0.35 ns	–0.17 ns
RIE	**–0.62**** (0.16 ns)	–0.15 ns	–0.18 ns	**–0.46***	0.01 ns	–0.05 ns	–0.16 ns	–0.01 ns	–0.36 ns	–0.15 ns
IRO	**0.65**** (0.20 ns)	0.22 ns	0.42 ns	0.13 ns	0.03 ns	–0.04 ns	–0.11 ns	–0.15 ns	0.06 ns	0.23 ns
IREOi	**0.66**** (0.32 ns)	0.35 ns	0.25 ns	0.06 ns	–0.04 ns	–0.15 ns	–0.06 ns	–0.20 ns	–0.27 ns	0.23 ns
IREOii	**0.68**** (0.23 ns)	0.37 ns	0.26 ns	–0.06 ns	0.12 ns	0.02 ns	–0.23 ns	0.02 ns	–0.16 ns	0.04 ns
IRNi	0.26 ns	0.23 ns	0.12 ns	0.17 ns	–0.01 ns	–0.21 ns	–0.32 ns	–0.31 ns	–0.30 ns	–0.41 ns
IRNii	0.29 ns	0.26 ns	–0.01 ns	0.18 ns	0.26 ns	0.06 ns	**–0.54***	–0.21 ns	–0.20 ns	0.31 ns
IRNiii	–0.24 ns	0.39 ns	–0.09 ns	0.27 ns	–0.15 ns	–0.14 ns	–0.31 ns	–0.11 ns	–0.15 ns	0.25 ns
IRSTi	**0.64**** (0.29 ns)	0.37 ns	0.26 ns	0.11 ns	–0.01 ns	–0.21 ns	–0.09 ns	–0.20 ns	–0.24 ns	0.26 ns
IRSTii	**0.64**** (0.18 ns)	0.39 ns	0.23 ns	–0.02 ns	0.12 ns	–0.02 ns	–0.31 ns	–0.03 ns	–0.14 ns	0.14 ns

Significant correlations highlighted in bold (*$P < 0.05$; **$P < 0.01$; ***$P < 0.001$; ns, not significant).

above). It is possible that the correlations between angular and spatial-packing variables given in Table 4 are an artefact of these strong growth-related trends rather than any real structural interaction. Partial correlations controlling for background changes in MQ were therefore computed and are given in parentheses in Table 4. In addition, residuals from plots against MQ were used in regression and rank coefficient calculations (Table 5). Comparisons that revealed both significant partial correlations and rank correlations between residuals were deemed to be free from background growth-related variances and to be representative of possible structural relationships between angular and spatial-packing variables.

The analyses revealed that there is a robust association between relative eye size (IRO) and the angle of orbital

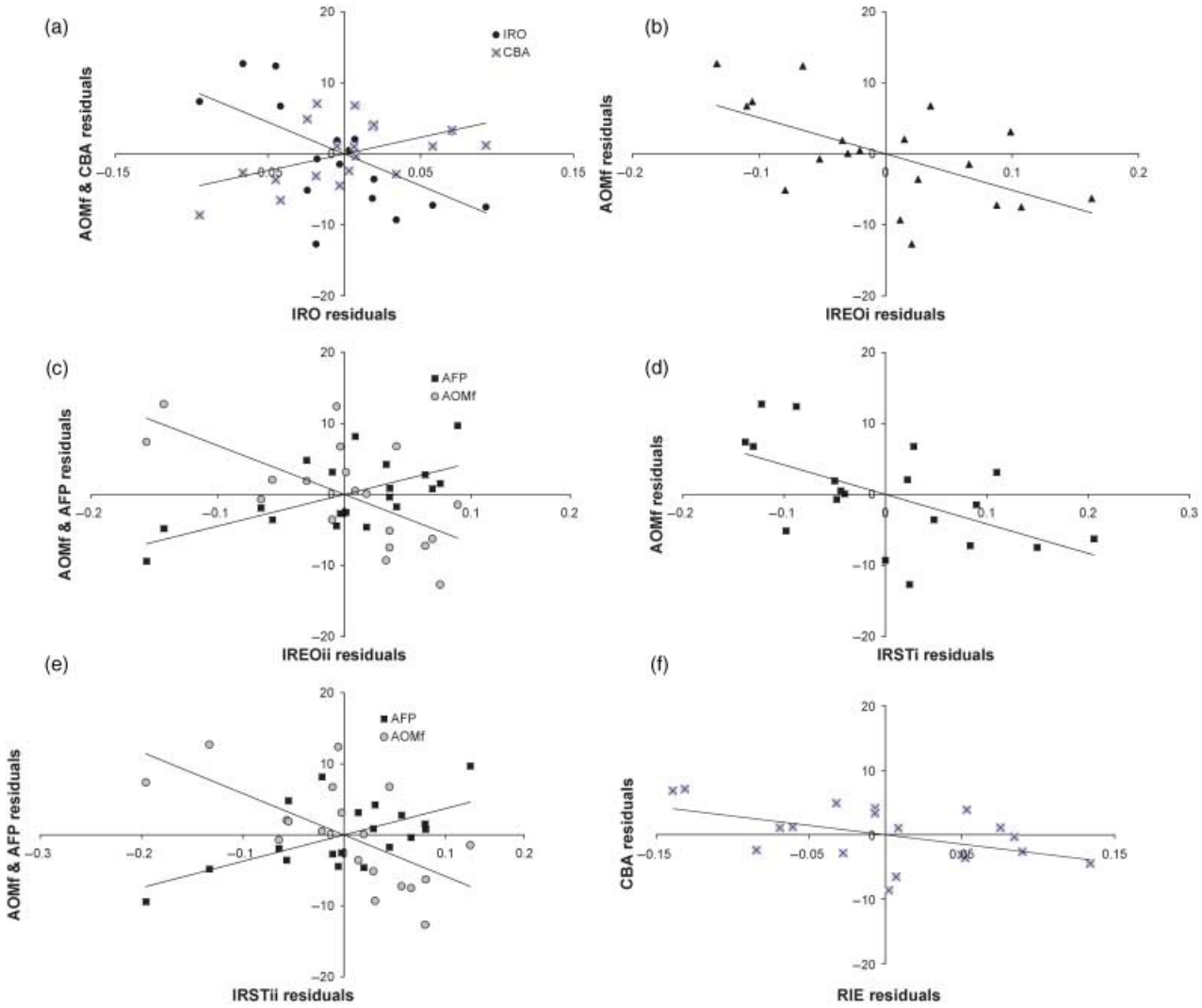

Fig. 11 Plots of residuals from comparisons against the maturation quotient (MQ): (a) angle of orbital margin frontation (AOMf) and cranial base angle (CBA) against relative eye size (IRO); (b) angle of orbital margin frontation (AOMf) against eye plus brain size relative to skull volume (IREOi); (c) angle of orbital margin frontation (AOMf) and angle of facial projection (AFP) against eye plus brain size relative to cranial base length (IREOii); (d) angle of orbital margin frontation (AOMf) against the combined soft-tissue size relative to skull volume (IRSTi); (e) angle of orbital margin frontation (AOMf) and angle of facial projection (AFP) against combined soft-tissue size relative to cranial base length (IRSTii); (f) cranial base angle (CBA) against infratentorial size relative to posterior cranial base length (RIE). Reduced major axes regressions are shown for each plot.

Table 7 Bivariate comparisons of the maturation quotient and spatial-packing variables that were significantly correlated with principal component scores after controlling for MQ-related changes (see Table 6)

	a	95% *a*	*b*
PC1 vs. MQ	0.0022	0.0016 > 0.0029	–0.1220
PC4 vs. RIE	–0.3755	–0.6967 > 0.3593	0.4285
PC7 vs. IRNii	–1.0534	–1.4520 > –0.7430	0.3127
PC9 vs. IRE	–0.4172	–0.5353 > –0.2828	0.3504

margin frontation (AOMf). This strong link is carried over to yield significant correlations in combination with the endocranial size in variables IREOi,ii and IRSTi,ii (Fig. 11a–e). These correlations are negative, i.e. orbital margin frontation is decreasing with increases of relative size. This is the opposite of the trend predicted by the hypotheses. Findings also demonstrate robust correlations of the angle of facial projection (AFP) against the size of the eyes plus endocranium relative to cranial base length (IREOii). Again, this link is carried over to yield correlations with IRSTii (Fig. 11c,e) and is

inconsistent with the decreases of facial prognathism predicted by the hypotheses. There were two significant rank correlations between residuals (Table 5) that had insignificant partial correlations (Table 4). These anomalies may simply reflect the differences between the statistical methods used or could suggest that after adjustment for fetal growth there may be a weak relationship of the cranial base angle (CBA) with RIE and IRO (Fig. 11a,f).

To test the hypotheses in terms of non-Euclidean shape, comparisons were made of the first ten principal component scores against spatial-packing variables. PC1 scores, which account for 32.2% of the total variance, significantly correlated with RIE, IRO, IREOi,ii and IRSTi,ii. These variables and PC1 scores also show strong correlations with MQ. To evaluate the compounding influence of growth, partial correlations were computed whilst controlling for MQ. These are given in parentheses in Table 6. The findings reveal that the 32.3% of the variation represented by PC1 is primarily related to growth of the fetus rather than any specific shape response to spatial packing. Significant growth-adjusted associations were observed between PC4 scores and RIE, PC7 scores and IRNii, and PC9 scores and IRE (Fig. 12a,b). Reconstructions for the plot of PC4 scores against RIE show that the orbital margins tilt to a more coronal, forward-facing position and that the hormion region decreases in relative size (Fig. 12a). Reconstructions for associations with PC7 and PC9 are also given in Fig. 12 (b,c). However, as the changes represented are so small (3.4 and 2.2% of total variance, respectively) it is unlikely that these reflect any major spatial-packing influence of the nasal septum and endocranial size.

Discussion

Tarsiers appear remarkably distinct by comparison with other extant primates. They possess unusually large eyes and share characteristics with both the strepsirhines and the anthropoid suborders. All this makes the genus particularly interesting for evaluating ideas concerning the influence of soft-tissue enlargement on skull architecture. One way to test such ideas against a backdrop of sufficient biological change that can outweigh any intraspecific noise is to examine tarsier development. Here we document for the first time growth-related changes of the fetal tarsier skull and test for the influence of brain, eye and nasal septum enlargement in shaping the skull.

Comparisons against the maturation quotient demonstrated several interesting trends. Both the bivariate and the shape analyses indicate that there is no significant change in convergence or frontation of the orbital axes, but that there are notable growth-related changes in the face, cranial base and position of the orbital margins. As the tarsier fetus matures the face projects further forward, the cranial base flattens out and the orbital margins shift forward to a more perpendicular position relative to the midsagittal plane (i.e. frontate). These findings are consistent with those from previous studies of primate fetuses (Jeffery & Spoor, 2002; Jeffery, 2003). However, the rate of cranial base retroflexion for the present tarsius sample (slope = 0.21) is noticeably less than that reported for fetal samples of *Macaca nemestrina* (0.28) and *Aloutta caraya* (0.43) (Jeffery, 2003). In studies of human samples, most of the convergence is reported to occur early in development, primarily during the late embryonic stages of life (Zimmerman et al. 1934; Sperber, 1981; Diewert, 1985). It is possible that similar late embryonic, early fetal orbital convergence was not sampled sufficiently in the present study. The youngest individual studied here was already 26% MQ.

Findings for base lengths against MQ show that increases of total base length are primarily due to the anterior base increasing at twice the rate of the posterior base. These findings are consistent with those documented for fetal samples of *Alouatta caraya*, *Macaca nemestrina* and *Homo sapiens* (Jeffery & Spoor, 2002; Jeffery, 2003). The nasal septum is shown here to have one of the slowest rates of growth against MQ (slope = 0.0046). Septal growth was comparable with that of the posterior base and a little greater than that of the infratentorial volume.

Overall increases of endocranial size were shown to be primarily due to supratentorial enlargement, corresponding to the diencephalon and the cerebrum. The rate of expansion is almost three times that for the infratentorial (i.e. cerebellum plus brainstem) compartment. Although in each specimen the combined volume of the eyes is less than that of the endocranium, the rate of eye growth against MQ is significantly greater than that for the endocranium. This indicates that eye size may exceed brain size following further postnatal development and supports earlier reports that the tarsier eyes are the same or greater than the size of the brain (Sprankel, 1965; Castenholz, 1984). This remarkable rate of fetal eye growth probably reflects

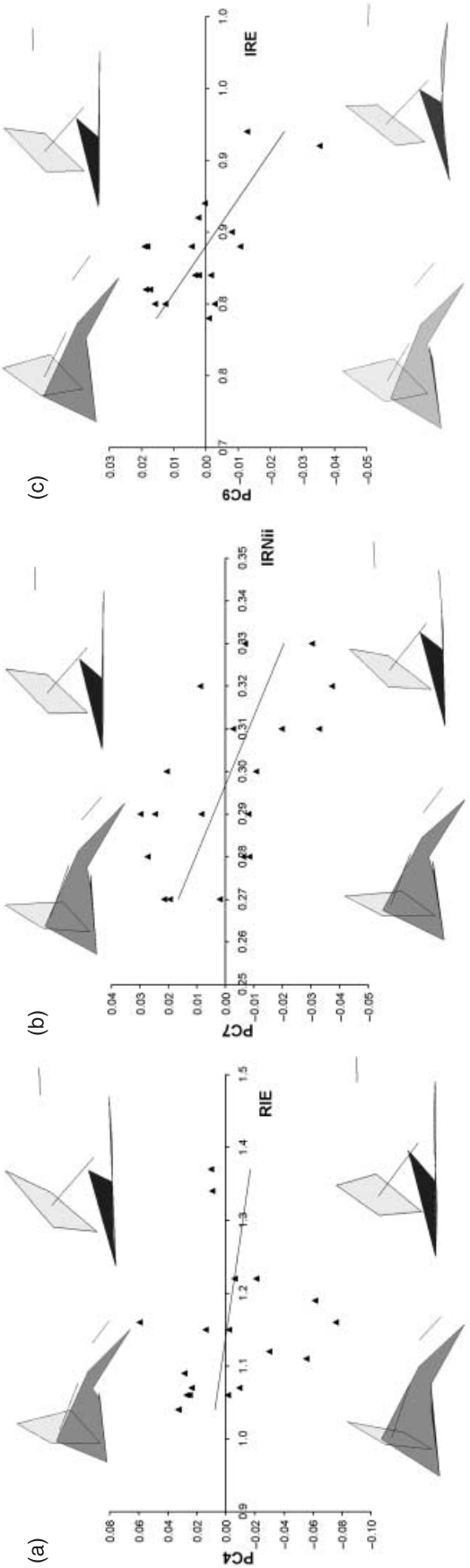

Fig. 12 Plot of principal component (PC) scores against spatial packing variables with wireframe reconstructions from the lateral and dorsal view showing the shape variations represented: (a) PC4 scores against infratentorial size relative to posterior cranial base length (RIE) demonstrating frontation of the orbital margins and relative reduction in the size of the hormion as RIE increases; (b) PC7 scores against nasal septum size relative to cranial base length (IRNii) showing a slight increase in the relative height of the nasal septum, particular around foramen ceacum (Fc); (c) PC9 scores against endocranial size relative to cranial base length (IRE) demonstrating a twisting of the midline basicranium. Note that components only represent 10.1, 3.4 and 2.2% of the total shape variance, respectively. Reduced major axes regression are also shown.

selection for visual adaptations (see Kay & Kirk, 2000; Collins et al. 2005). The rate of endocranial enlargement in the present tarsier sample (slope = 0.12) is less than half that for fetal samples of *Macaca nemestrina* (0.45) and *Aloutta caraya* (0.38) (Jeffery, 2003). The same is also true for increases of the supratentorial volume (0.12, 0.44 and 0.37, respectively) and for increases of infratentorial volume (0.04, 0.17 and 0.16, respectively). Overall, growth of the tarsier fetus occurs at about half the rate of that observed for *Macaca* and *Alouatta* (Jeffery, 2003).

Taking into account the above growth-related changes allows for robust testing of the spatial-packing hypotheses outlined in the introduction. To support the hypotheses the correlations of relative sizes should be statistically significant and negative for growth-adjusted comparisons with cranial base angle (basicranial flexion), facial projection angle (reduction of facial prognathism), and the angles of orbital axes and margin convergence as well as the angle of orbital axes frontation. The correlation with the angle of orbital margin frontation should be positive and statistically significant.

There is little evidence from the findings reported here to support the hypotheses that relative enlargement of the nasal septum, enlargement of the endocranial volume relative to base length or enlargement of the supratentorial volume relative to the anterior cranial base length influences cranial base angulation, orbit orientation or facial projection. There is weak evidence from the bivariate and shape analyses to suggest that flattening of the cranial base may be associated with decreases of the infratentorial volume relative to the length of the posterior cranial base. However, this is the opposite of the trend predicted. The base is shown to retroflex towards the infratentorial region rather than away from it. This could be due to the observed reduction of relative infratentorial size allowing the faster growing posterior base to retroflex towards the posterior cranial fossa. Nevertheless, the results do not support the hypothesis that relative infratentorial enlargement drives flexion of the cranial base, orbit reorientation or facial recession. There is also weak evidence of an association between orbit size relative to skull size and cranial base angle, but again this does not appear to follow the predicted pattern. However, a more robust association was observed between relative eye size and orbital margin frontation. This strong association can be seen throughout comparisons with relative eye plus brain size and also with the combined relative soft-tissue sizes. Together with the brain, the relative expansion of the eyes also appears to influence the angle of facial projection. These findings suggest that as the eyes and brain increase in relative size, the margins of the orbits frontate and the face gradually becomes more prognathic.

In summary, we can reject the hypothesis that relative enlargement of the nasal septum significantly influences skull development. Furthermore, given results from this and previous studies (Jeffery & Spoor, 2002; Jeffery, 2003) we can also reject the hypothesis that relative brain enlargement is a significant factor. However, findings appear to support the hypothesis that eye enlargement, as well as the effects of eye enlargement combined with those of other soft tissues, can influence tarsier skull development, particularly orbital frontation.

It is important to note that several other soft-tissue components not investigated in the present study could also have had a significant influence. For instance, the reduction in the size of the olfactory bulbs, which has been used to link the tarsiers with the anthropoid primates, may have had a significant influence on the cranial base and interorbital architecture. In addition, changes to the cortical vs. non-cortical parts of the brain have also been proposed as an influence on basicranial morphology (Strait, 1999). These and similar ideas warrant further consideration in any future investigations of the spatial-packing hypotheses.

The finding that cranial base angle is independent of relative brain size corroborates results from two previous fetal studies (Jeffery & Spoor, 2002; Jeffery, 2003). The cranial base appears to flatten out (retroflex) during fetal development in *Homo sapiens*, *Alouatta caraya*, *Macaca nemestrina* and *T. bancanus* despite massive increases of absolute brain size, and in some cases marked increases of relative brain size too. These findings indicate that brain expansion is not the primary driving force behind basicranial flexion. However, this does not preclude the interesting possibility that brain expansion tempers or limits the extent of basicranial retroflexion determined morphogenetically (Lieberman et al. 2000; Gould, 2002; Ross et al. 2004). Presumably the outcome of such constraining interactions between bony and soft tissues would be determined by the relative growth capacity (product of the rate and mass of growing tissue divided by skull size) of the tissues involved. Thus, for instance, if growth of the bony component is greater, then the expression of the soft-tissue

morphogenetic template is constrained and the soft tissue moulds itself to the bony morphology. If growth capacities are equal then expression of both morphogenetic templates are curbed and the outcome appears quiescent. However, if the soft-tissue growth has a greater potential, then the expression of the bony morphogenetic template will be physically constrained instead. Thinking in these terms may help explain why studies of adult primates reveal strong statistical links between basicranial angulation and relative brain size whereas studies of primate fetuses do not (compare Ross & Ravosa, 1993; Spoor, 1997; Jeffery & Spoor, 2002; Jeffery, 2003; Ross et al. 2004). The discrepancy could arise because the fetal studies document the process of constraint within a species whereas the adult studies demonstrate species differences in the end points at which basicranial retroflexion was halted by brain expansion. In reality, the interaction among tissues is likely to be more complicated than depicted here. It would involve, for example, other tissues such as the upper respiratory tract constraining the extent of basicranial flexion later in postnatal human development (see Ross et al. 2004; Jeffery, 2005). Consequently, the next challenge is to work out whether the proposed effects of developmental constraint can be observed among other tissue types and to determine if the effects of relative eye enlargement are unique to tarsiers or can be found in primate species with smaller eyes.

Acknowledgements

Our thanks go to Miss Natasha Russell and Miss Lauren Moore for assisting with the image analyses, Dr Philip Cox for comments on an earlier draft of this manuscript, and the Hubrecht Collections, Netherlands, for providing the specimens for study. We also thank Professor Dan Lieberman and two anonymous referees for comments that greatly improved this paper. This research was partly funded by the University of Liverpool Research Development Fund (grant no. 4361) and partly supported by a Biotechnology and Biological Sciences Research Council grant (no. BB/D000068/1).

References

Adamopoulos G, Tassopoulos G, Ferekydis E, Bosinakou M, Kontozoglou TE (1994) Nasomaxillary skeletal dimensions complex in patients with osseous nasal septum deformities. *J Otolaryngol* **23**, 84–87.

Barton RA (2004) From the cover: binocularity and brain evolution in primates. *Proc Natl Acad Sci USA* **101**, 10113–10115.

Bastir M, Rosas A (2005) Hierarchical nature of morphological integration and modularity in the human posterior face. *Am J Phys Anthropol* **128**, 26–34.

Beard KC, Krishtalka L, Stucky RK (1991) First skulls of the early Eocene primate *Shoshonius cooperi* and the anthropoid-tarsier dichotomy. *Nature* **349**, 64–67.

Biegert J (1963) The evaluation of characters of the skull, hands and feet for primate taxonomy. In *Classification and Human Evolution* (ed. Washburn, SL), pp. 116–145. Chicago: Aldine.

Bloch JI, Silcox MT (2006) Cranial anatomy of the Paleocene plesiadapiform *Carpolestes simpsoni* (Mammalia, Primates) using ultra high-resolution X-ray computed tomography, and the relationships of plesiadapiforms to Euprimates. *J Human Evol* **50**, 1–35.

Bookstein F (1992) *Morphometric Tools for Landmark Data: Geometry and Biology*. Cambridge: Cambridge University Press.

Bukovic D Jr, Radionov D, Verzak Z, Lulic-Dukic O, Azinovic Z, Bagic I (1997) Effect of unilateral function on craniofacial growth. *Collegium Antropologicum* **21**, 217–228.

Carlson DS (1985) *Introduction to Craniofacial Biology*. Ann Arbor, MI: University of Michigan.

Cartmill M (1974) Rethinking primate origins. *Science* **184**, 436–443.

Cartmill M (1978) The orbital mosaic in prosimians and the use of variable traits in systematics. *Folia Primatol* **30**, 89–114.

Castenholz A (1984) The eye of *Tarsius*. In *Biology of Tarsiers* (ed. Niemitz, C), pp. 303–318. Stuttgart: Gustav Fischer.

Ciochon RL, Gunnell GF (2002) Chronology of primate discoveries in Myanmar: influences on the anthropoid origins debate. *Am J Phys Anthropol Suppl* **35**, 2–35.

Collins CE, Hendrickson A, Kaas JH (2005) Overview of the visual system of Tarsius. *Anat Record Part A, Discoveries Mol Cell Evol Biol* **287**, 1013–1025.

Copray JC (1986) Growth of the nasal septal cartilage of the rat in vitro. *J Anat* **144**, 99–111.

De Beer G (1985) *The Development of the Vertebrate Skull*. Chicago: University of Chicago Press.

Diewert VM (1985) Development of human craniofacial morphology during the late embryonic and early fetal periods. *Am J Orthod* **88**, 64–76.

Dubois E (1869) On the *Pithecanthropus erectus*: a transitional form between Man and the Apes. *J Anthropol Inst Great Britain Ireland* **25**, 240–255.

Duterloo HS, Enlow DH (1970) A comparative study of cranial growth in *Homo* and *Macaca*. *Am J Anat* **127**, 357–368.

Enlow DH, Hunter WS (1968) The growth of the face in relation to the cranial base. *Rep Congr Eur Orthod Soc* **44**, 321–335.

Enlow DH, McNamara JA (1973) The neurocranial basis for facial form and pattern. *Angle Orthod* **43**, 256–270.

Enlow DH (1990) *Facial Growth*. Philadelphia: Saunders.

Ford EHR (1956) The growth of the foetal skull. *J Anat* **90**, 63–72.

Glanville EV (1969) Nasal shape, prognathism and adaptation in man. *Am J Phys Anthropol* **30**, 29–37.

Gould SJ (1977) *Ontogeny and Phylogeny*. London: Harvard University Press.

Gould SJ, Lewontin RC (1979) The spandrels of San Marco and the Panglossian paradigm: a critique of the adaptationist programme. *Proc R Soc Lond B Biol Sci* **205**, 581–598.

Gould SJ (2002) *The Structure of Evolutionary Theory*. Boston: Harvard University Press.

Hans MG, Scaletta L, Occhino JC (1996) The effects of antirat nasal septum cartilage antisera on facial growth in the rat. *Am J Orthodontics Dentofacial Orthopedics* **109**, 607–615.

Heesy CP (2004) On the relationship between orbit orientation and binocular visual field overlap in mammals. *Anat Record Part A, Discoveries Mol Cell Evol Biol* **281**, 1104–1110.

Huxley TH (1861) On the zoological relations of man with the lower animals. *Natural History Rev* **1**, 67–84.

Jeffery N (1999) *Fetal Development and Evolution of the Human Cranial Base Anatomy and Developmental Biology*. London: University College.

Jeffery N (2002) Differential regional brain growth and rotation of the prenatal human tentorium cerebelli. *J Anat* **200**, 135–144.

Jeffery N, Spoor C (2002) Brain size and the human cranial base: a prenatal perspective. *Am J Phys Anthropol* **118**, 324–340.

Jeffery N (2003) Brain expansion and comparative prenatal ontogeny of the non-hominoid primate cranial base. *J Hum Evol* **45**, 263–284.

Jeffery N, Spoor C (2004) Ossification and midline shape changes of the human fetal cranial base. *Am J Phys Anthropol* **123**, 78–90.

Jeffery N (2005) Cranial base angulation and growth of the human fetal pharynx. *Anatt Rec* **284A**, 491–499.

Jeffery N, Spoor C (2006) The primate subarcuate fossa and its relationship to the semicircular canals part I: prenatal growth. *J Hum Evol* **51**, 537–549.

Kay RF, Cartmill M (1977) Cranial morphology and adaptations of Palaechthon nacimienti and other Paromomyidae (Plesiadapoidea, ?Primates), with a description of a new genus and species. *J Hum Evol* **6**, 19–35.

Kay RF, Ross C, Williams BA (1997) Anthropoid origins. *Science* **275**, 797–804.

Kay RF, Kirk EC (2000) Osteological evidence for the evolution of activity pattern and visual acuity in primates. *Am J Phys Anthropol* **113**, 235–262.

Kirk EC (2006) Effects of activity pattern on eye size and orbital aperture size in primates. *J Human Evol* **51**, 159–170.

Koski K (1968) Cranial growth centers: facts of fallacies? *Am J Orthodontics* **54**, 566–583.

Kvinnsland S (1970) The relationship between the cartilaginous nasal septum and maxillary growth during human fetal life. *Cleft Palate J* **7**, 523–532.

Kvinnsland S (1974) Partial resection of the cartilaginous nasal septum in rats; its influence on growth. *Angle Orthodontist* **44**, 135–140.

Le Gros Clark WE (1934) *Early Forerunners of Man: A Morphological Study of Evolutionary Origin of the Primates*. Baltimore: William Wood.

Lieberman DE, Ross CF, Ravosa MJ (2000) The primate cranial base: ontogeny, function, and integration. *Am J Phys Anthropol Suppl* **31**, 117–169.

Lozanoff S, Doll S, Hallgrimsson B, Neufeld E (2004) Prenatal growth of the interorbital septum in *Macaca mulatta*. *Ann Anat* **186**, 435–442.

McCarthy RC, Lieberman DE (2001) Posterior maxillary (PM) plane and anterior cranial architecture in primates. *Anat Rec* **264**, 247–260.

Meijering EH, Niessen WJ, Viergever MA (2001) Quantitative evaluation of convolution-based methods for medical image interpolation. *Med Image Anal* **5**, 111–126.

Miller ER, Gunnell GF, Martin RD (2005) Deep time and the search for anthropoid origins. *Am J Phys Anthropol Suppl* **41**, 60–95.

Moss ML, Young RW (1960) A functional approach to craniology. *Am J Phys Anthropol* **18**, 281–292.

Moss ML, Bromberg BE, Song IC, Eisenmann G (1968) The passive role of nasal septal cartilage in mid-facial growth. *Plastic Reconstructive Surg* **41**, 536–542.

Moss ML (1997a) The functional matrix hypothesis revisited. 3. The genomic thesis. *Am J Orthodontics Dentofacial Orthopedics* **112**, 338–342.

Moss ML (1997b) The functional matrix hypothesis revisited. 4. The epigenetic antithesis and the resolving synthesis. *Am J Orthodontics Dentofacial Orthopedics* **112**, 410–417.

Noble VE, Kowalski EM, Ravosa MJ (2000) Orbit orientation and the function of the mammalian postorbital bar. *J Zool Soc London* **250**, 405–418.

O'Higgins P, Jones N (1998) Facial growth in *Cercocebus torquatus*: an application of three- dimensional geometric morphometric techniques to the study of morphological variation. *J Anat* **193**, 251–272.

O'Higgins P (2000a) Quantitative approaches to the study of craniofacial growth and evolution: advances in morphometric techniques. In: *Development, Growth and Evolution: Implications for the Study of the Hominid Skeleton* (eds O'Higgins P, Cohn, MJ), pp. 164–183. London: Academic Press.

O'Higgins P (2000b) The study of morphological variation in the hominid fossil record: biology, landmarks and geometry. *J Anat* **197**, 103–120.

Ravosa MJ, Noble VE, Hylander WL, Johnson KR, Kowalski EM (2000) Masticatory stress, orbital orientation and the evolution of the primate postorbital bar. *J Human Evol* **38**, 667–693.

Ravosa MJ, Savakova DG (2004) Euprimate origins: the eyes have it. *J Hum Evol* **46**, 357–364.

Richardson MK, Narraway J (1999) A treasure house of comparative embryology. *Int J Dev Biol* **43**, 591–602.

Ronning O, Kantomaa T (1985) Experimental nasal septum deviation in the rat. *Eur J Orthodontics* **7**, 248–254.

Ross CF (1993) *The Function of the Postorbital Septum and Anthropoid Origins Biological Anthropology and Anatomy*. Durham, NC: Duke University.

Ross CF, Ravosa MJ (1993) Basicranial flexion, relative brain size, and facial kyphosis in nonhuman primates. *Am J Phys Anthropol* **91**, 305–324.

Ross CF (1995) Allometric and functional influences on primate orbit orientation and the origins of Anthropodea. *J Human Evol* **29**, 201–227.

Ross C (1996) Adaptive explanation for the origins of the Anthropoidea (Primates). *Am J Primatol* **40**, 205–230.

Ross C, Williams B, Kay RF (1998) Phylogenetic analysis of anthropoid relationships. *J Human Evol* **35**, 221–306.

Ross CF, Henneberg M, Ravosa MJ, Richard S (2004) Curivilinear, geometric and phylogenetic modeling of basicranial flexion: is it adaptive, is it cronstrained? *J Human Evol* **46**, 185–213.

Ross CF, Kay RF (2004) Anthropoid origins: retrospective and prospective. In *Anthropoid Origins: New Visions* (eds Ross CF, Kay RF), pp. 699–737. New York: Plenum.

Rossie JB, Ni X, Beard KC (2006) Cranial remains of an Eocene tarsier. *Proc Natl Acad Sci USA* **103**, 4381–4385.

Rutimeyer L (1871) On the difference in the cranial structure of the gorilla, chimpanzee, and orang-outang, with special reference to sex and age, and with some remarks on the Darwinian theory. *J Anthropol* **1**, 268–277.

Sarnat BG (1978) Differential craniofacial skeletal changes after postnatal experimental surgery in young and adult animals. *Ann Plastic Surg* **1**, 131–145.

Sarnat BG (1982) Eye and orbital size in the young and adult. Some postnatal experimental and clinical relationships. *Ophthalmologica* **185**, 74–89.

Schultz AH (1935) The nasal cartilages in higher primates. *Am J Phys Anthropol* **20**, 205–212.

Schultz AH (1940) The size of the orbit and the eye in primates. *Am J Phys Anthropol* **26**, 398–408.

Schwartz JH (2003) How close are the similarities between Tarsius and other primates? In *Tarsiers: Past, Present and Future* (eds Wright PC, Simons EL, Gursky S), pp. 50–96. Piscataway, NJ: Rutgers University Press.

Scott JH (1953) The cartilage of the nasal septum (a contribution to the study of facial growth). *Br Dental J* **95**, 37–43.

Scott JH (1958) The cranial base. *Am J Phys Anthropol* **16**, 319–348.

Simons EL, Rasmussen DT (1989) Cranial morphology of *Aegyptopithecus* and *Tarsius* and the question of the tarsier-anthropoidean clade. *Am J Phys Anthropol* **79**, 1–23.

Sperber GH (1981) *Craniofacial Embryology*. Bristol: Wright PSG.

Spoor F (1997) Basicranial architecture and relative brain size of Sts 5. (*Australopithecus africanus*) and other Plio-Pleistocene hominids. *South African J Sci* **93**, 182–187.

Sprankel H (1965) Untersuchungen an Tarsius. I. Morphologie des Schwanzes nebst ethologischen Bemerkungen. *Folia Primatol* **3**, 153–188.

Strait DS (1999) The scaling of basicranial flexion and length. *J Hum Evol* **37**, 701–719.

Streeter GL (1920) Weight, sitting height, headsize, foot length, and menstraul age of the human. *Contrib Embryol* **55**, 143–159.

Szalay FS, Wilson JA (1976) Basicranial morphology of the early tertiary tarsiiform Rooneyia from Texas. *Folia Primatol* **25**, 288–293.

Verwoerd CD, Urbanus NA, Nijdam DC (1979) The effects of septal surgery on the growth of nose and maxilla. *Rhinology* **17**, 53–63.

Verwoerd CD, Urbanus NA, Mastenbroek GJ (1980) The influence of partial resections of the nasal septal cartilage on the growth of the upper jaw and the nose: an experimental study in rabbits. *Clin Otolaryngol Allied Sci* **5**, 291–302.

Weidenreich F (1941) The brain and its role in the phylogenetic transformation of the human skull. *Trans Am Phil Soc* **31**, 321–442.

Wharton CH (1950) The Tarsier in captivity. *J Mammal* **31**, 260–268.

Zimmerman AA, Armstrong EL, Scammon RE (1934) The change in the position of the eyeballs during fetal life. *Anat Rec* **59**, 109–134.